Surface Review and Letters, Vol. 3, No. 1 (1996) 765–769

NOVEL STRUCTURES FROM ARC-VAPORIZED CARBON AND METALS: SINGLE-LAYER CARBON NANOTUBES AND METALLOFULLERENES

C.-H. KIANG,* P. H. M. VAN LOOSDRECHT, R. BEYERS,
J. R. SALEM, and D. S. BETHUNE
IBM Almaden Research Center, 650 Harry Road, San Jose, CA 95120, USA

W. A. GODDARD III
Materials and Molecular Simulation Center,
Division of Chemistry and Chemical Engineering,
California Institute of Technology, Pasadena, CA 91125, USA

H. C. DORN, P. BURBANK, and S. STEVENSON
Department of Chemistry, Virginia Polytechnic Institute and State University,
Blacksburg, VA 24061, USA

By covaporizing metals with carbon in a fullerene generator, diverse fullerene-related structures can be produced. Adding cobalt to the graphite anode leads to the production of single-layer carbon nanotubes. We find that the relative abundance of tubes with different diameters can be successfully altered by the presence of various catalyst promoters such as sulfur, bismuth, or lead. If Sc is covaporized in the arc, many Sc-containing metallofullerenes form abundantly. Purified $Sc_3@C_{82}$ has been obtained by HPLC techniques, and its dynamics have been investigated using electron paramagnetic resonance spectroscopy. The unusually large, strongly temperature-dependent linewidths and the temperature-dependent hyperfine coupling suggest that the Sc atoms form a trimer which rapidly reorients within the C_{82} cage.

1. Introduction

Atomic carbon vapor in an inert-gas environment self-assembles into sp^2 bonded, nanometer-scale networks: the fullerenes. The addition of metal to the electric arc leads to the production of new classes of fullerene-related materials. For example, Fe, Co, and Ni have been found to catalyze the growth of nanometer diameter single-layer carbon nanotubes,[1–3] one or more metal atoms can be incarcerated in fullerene cages to give metallofullerenes,[4] and nanocrystals of metal or metal carbides such as YC_2 can be enclosed in layers of graphene sheet providing nanoparticles encapsulated in graphitic polyhedra.[5] Metal/carbon mixed cage structures called metallocarbohedrenes have also been reported.[6] In the first part of this contribution we focus on the production of single-wall carbon nanotubes and the effects of the addition of catalyst promoters, and in the second part we describe a systematic study of the electron paramagnetic resonance (EPR) spectrum of $Sc_3@C_{82}$ for temperatures varying from 77 to 333 K.

2. Single-Layer Carbon Nanotubes

To understand the nanotube growth process and to design efficient methods to fabricate these materials, we studied the production of nanotubes under various conditions. The chamber atmosphere as well as the elements present in the carbon rods were modified. The experimental procedures are similar to

*Also affiliated with the Materials and Molecular Simulation Center.

those described previously.[2,7] In brief, we generated an arc between two electrodes under helium buffer gas. The 6-mm graphite anode was drilled with a 4-mm diameter hole, and was filled with a mixture of powdered Co, graphite and catalyst promoters such as S, Bi, and Pb. The anodes were vaporized with a DC current of 75–95 A, at a supply voltage of 20–25 V, under 300–500 Torr helium, with a flow rate of 5–15 ml/sec. Samples for transmission electron microscopy (TEM) studies were prepared by sonicating the soot in ethanol. A drop of the solvent containing suspended materials was then put on a holey carbon grid.

Figure 1(a) is a micrograph of soot containing a high density of single-layer nanotubes. These nanotubes are often curled [Fig. 1(b)], and also have a tendency to bundle together. Some tubes shown here are individual, clean nanotubes while others are covered with carbon and fullerene soot.

Many metal-containing clusters encapsulated in graphite-like polyhedra were found in the soot collected from the chamber walls. These particles formed abundantly when sulfur was introduced in the arc plasma, and had structures similar to particles found earlier in cathode deposits.[5] These filled polyhedra apparently form in the gas phase, implying that an intense electric field is not required during their formation. This feature may facilitate development of more time- and cost-effective ways to fabricate these materials. The magnetic properties

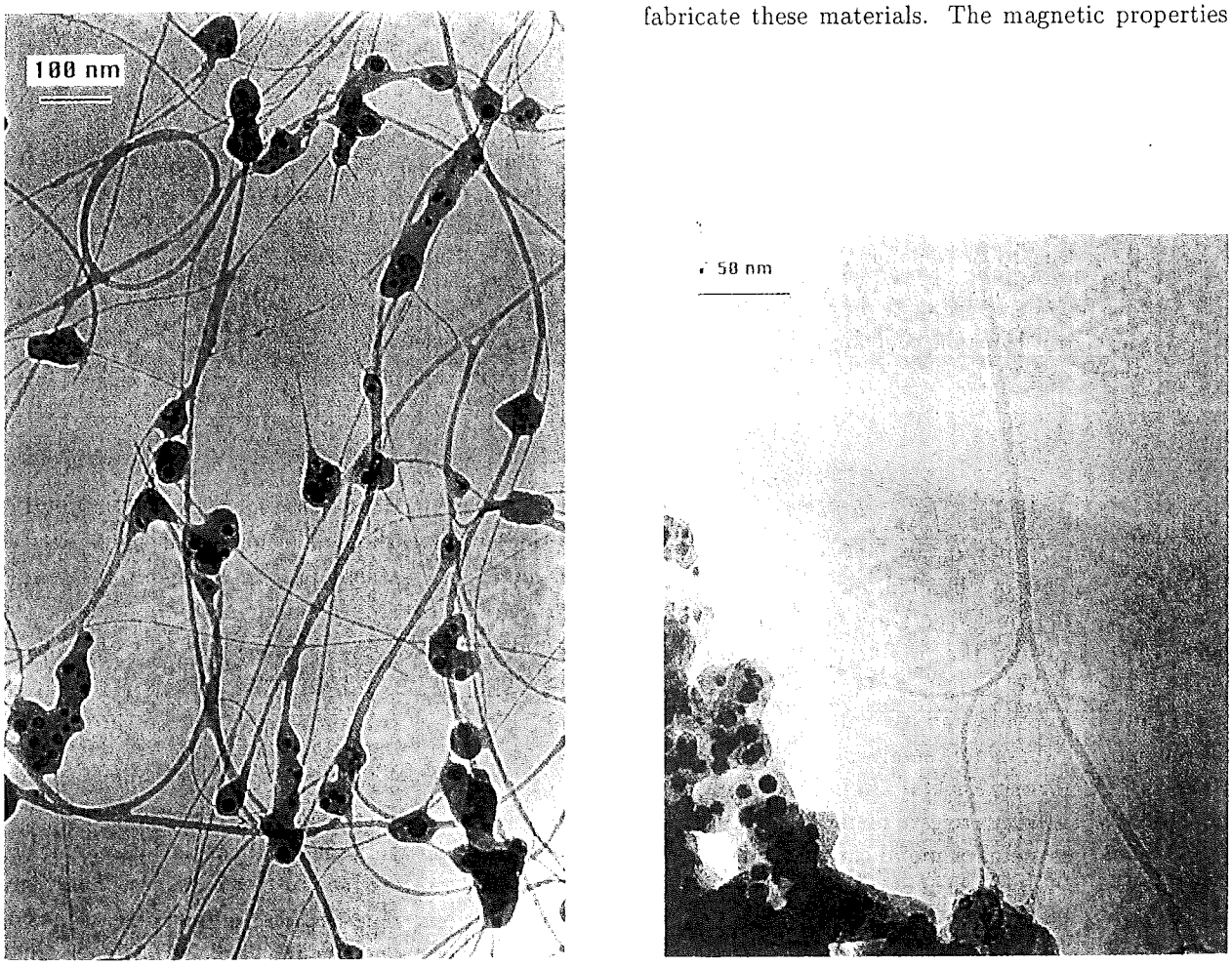

(a) (b)

Fig. 1. (a) Typical transmission electron micrograph of single-layer nanotubes in a soot sample made with cobalt, sulfur, and carbon. (b) Single-layer carbon nanotubes at higher magnification. Unlike the multilayer nanotubes found in the cathode deposit, these tubes are often bent.

of encapsulated Co clusters may lead to their use in applications of significant technological importance.[8]

The first step toward understanding the formation of these catalytically grown nanotubes is to locate the region where the reactions occur and to identify the catalytic species. To this end, we found that the soot deposited on the chamber wall contains only single-shell carbon nanotubes, whereas no single-layer carbon nanotubes were found in the cathode deposit. This is consistent with the postulate that these single-shell nanotubes nucleate and grow in the gas phase, unlike the multilayer nanotubes that form on the graphite cathode surface.[9] No definite association of nanotubes with the large cobalt particles can be discerned in the TEM micrographs, in contrast to the case of vapor-grown carbon fiber (VGCF).[10] This, together with the result that loading with more than 10 atomic % Co metal reduced the nanotube yield, is consistent with the hypothesis that small Co or Co carbide clusters (neutral or ionic) are the active catalyst. In this picture, too much Co would favor rapid growth of large Co clusters and reduce the number of small clusters available to catalyze the nanotube growth.

We studied the effect of the presence of additional elements on the formation of Co-catalyzed nanotubes. We found that several elements, including S, Bi, and Pb, can alter the relative abundance of nanotubes with different diameters. These promoters not only increased the yields of nanotubes, but also produced larger diameter tubules than were formed without them. These elements, however, do not catalyze nanotubes without Co. They only promote the reaction in the presence of a suitable catalyst. The diameters of nanotubes produced with Fe, Co, or Ni are between 1 nm and 2 nm. In contrast, large diameter (2–6 nm) single-layer nanotubes form abundantly with the addition of promoters such as S, Bi, and Pb. Figure 2 depicts the diameter range of the tubes produced with different promoters. The uncertainty in the diameters for the tubes with diameters larger than 2 nm is higher because they exhibit radial deformation. Figure 3 shows a histogram of tube abundance versus diameter, binned in 0.2-nm intervals. The histogram shows an oscillation of the abundance as a function of tube diameter. The abundance histogram shifts when a promoter is present, which suggests that the abundance of different size nanotubes

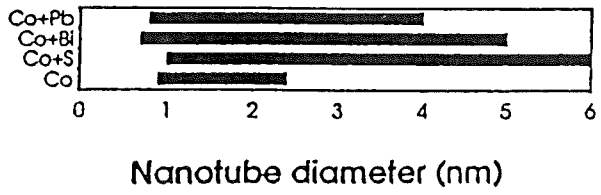

Fig. 2. Ranges of nanotube diameters produced by using Co catalyst with different promoters.

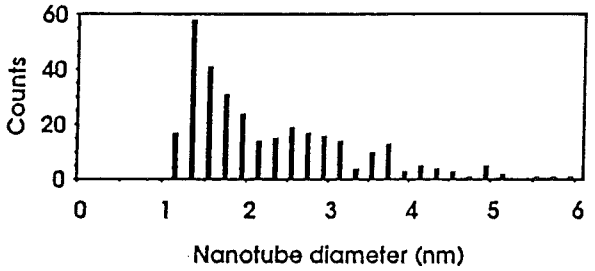

Fig. 3. Histogram of diameter distribution of single-layer carbon nanotubes produced by using Co and S promoter.

may be controlled by growth kinetics rather than energetics.[11] By studying the configuration of nanotubes produced via various catalysts and promoters, we hope to gain information on the formation mechanism of these exotic materials.

3. $Sc_3@C_{82}$ EPR

$Sc_3@C_{82}$ samples were obtained from soot produced by arc-burning cored graphite rods packed with a mixture of powdered graphite and scandium oxide and purified using high-performance liquid-chromatography separation with online EPR detection.[12,13] EPR spectra were recorded using dilute, degassed solutions of $Sc_3@C_{82}$ in decaline, sealed in a quartz tube.

Figure 4(a) shows an EPR spectrum of $Sc_3@C_{82}$ in supercooled decaline at $T = 193$ K. The 22-line spectrum, similar to those reported in the literature,[14] shows isotropic hyperfine coupling of an unpaired spin to three equivalent $I = 7/2$ Sc nuclei. The dashed line in Fig. 4(a) is the envelope of a simulated spectrum for such a system.

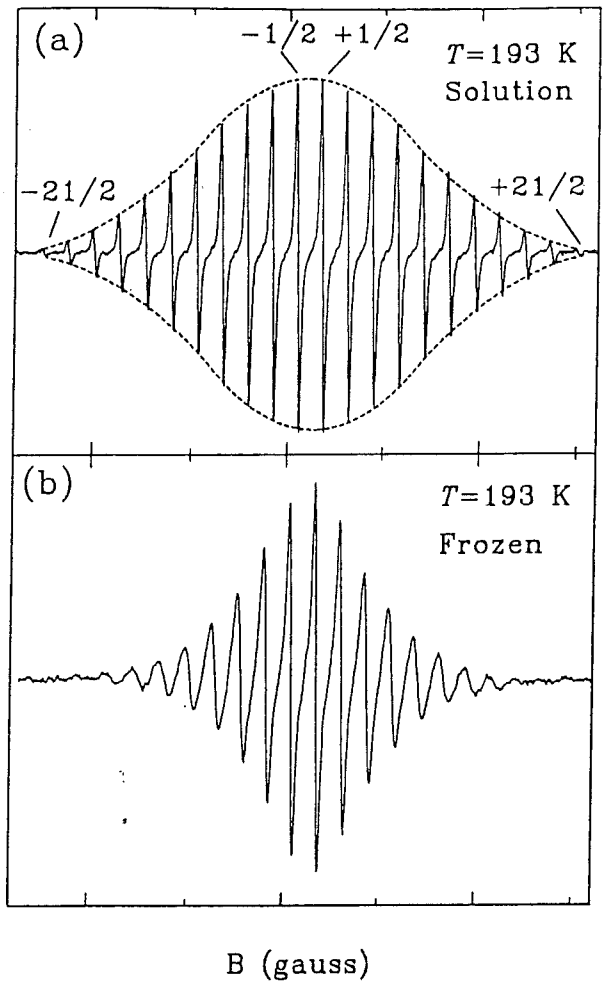

Fig. 4. EPR spectrum of $Sc_3@C_{82}$ in (a) fluid and (b) frozen decaline at $T = 193$ K. Some of the nuclear magnetic quantum numbers of the states involved in the transitions are indicated in (a). The dashed line is the envelope of a simulation of the fluid spectrum.

A striking feature of the room-temperature $Sc_3@C_{82}$ spectrum is the rather large width of the lines, ~0.8 gauss, more than an order of magnitude greater than the linewidths found for $Sc@C_{82}$, for instance.[15] In order to get a better understanding of this anomalously large linewidth, we studied the temperature dependence of the EPR spectrum. Figure 5 shows the temperature dependence of the linewidth of the $m_i = 1/2$ line both in frozen (solid circles) and liquid decaline (open circles). The linewidth has the qualitative temperature dependence expected for a paramagnetic species tumbling in solution due to

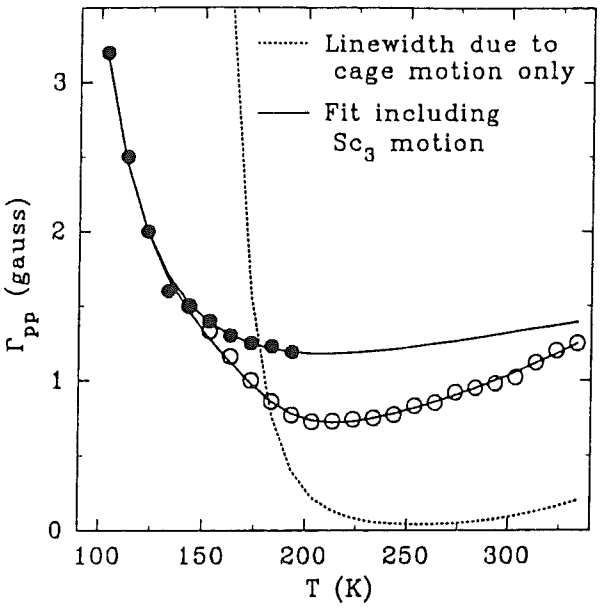

Fig. 5. Temperature dependence of the linewidth (Γ_{pp}) of the $m_i = +1/2$ (see Fig. 4) EPR transitions for $Sc_3@C_{82}$ in frozen (filled circles) and fluid (open circles) decaline. The dotted line is calculated assuming only cage motion. The solid line is a fit to a model including motion of both the cage and of the Sc atoms within the cage.

Brownian motion. For such a species the linewidth increases at low temperatures due to insufficient averaging of the magnetic anisotropy by reorientational motions, whereas at high temperatures the linewidth increases due to the interactions between the unpaired spin and the magnetic moment associated with rapid molecular rotation. However, *quantitatively* the temperature dependence strongly deviates from that expected for a C_{82} cage tumbling due to Brownian motion, as shown by the dotted line in Fig. 5. At high temperatures the linewidth is clearly too large, whereas at low temperatures it is seen to be too small. Even in the frozen decaline matrix, resolved hyperfine structure persists, as shown in Fig. 4(b), indicating there still is rapid reorientational averaging.

We are thus led to consider other broadening mechanisms. As discussed in Ref. 16, we conclude that the additional broadening results from motion of the Sc trimer within the fullerene cage. In brief, we postulate that the metal trimer can reorient by overcoming a barrier to rotation E_{Sc}, resulting

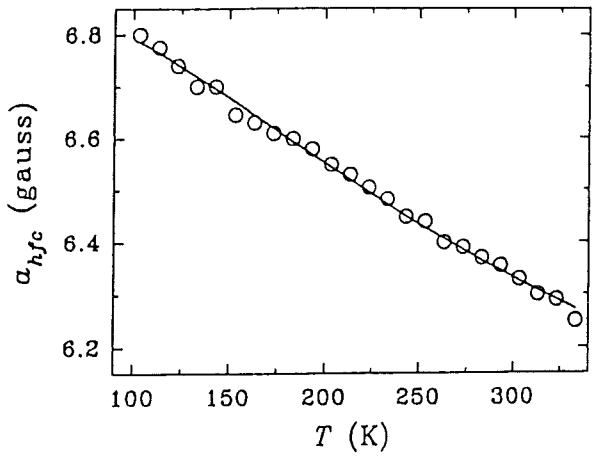

Fig. 6. Temperature dependence of the nuclear hyperfine coupling observed for $Sc_3@C_{82}$ in liquid and frozen decaline. The solid line is a fit to the data assuming Sc motion with respect to the C_{82} cage.

in a correlation time for trimer reorientation $\propto\exp(E_{\rm Sc}/kT)$. The solid lines in Fig. 5 are obtained by fitting this model to the data, yielding a value $E_{\rm Sc} = 28$ meV. An additional consequence of the Sc_3 reorientational motion is that the hyperfine coupling, $a_{\rm hfc}$, will be modulated as the trimer moves. The observed hyperfine coupling will be an averaged value, and will depend on the temperature. Figure 6 indeed shows the strong temperature dependence of $a_{\rm hfc}$, which varies by 10% over the range from 100 to 325 K. This evidence of large-amplitude motion strongly supports the notion of facile Sc trimer reorientation. In addition to the temperature dependence of the hyperfine coupling, the Sc_3 reorientations also leads to an m_i-dependent linewidth, as shown by the increasing broadening with increasing m_i in Fig. 4(b).

To summarize, single-layer nanotubes can be grown catalytically in high yield. One can greatly modify the size distribution by choosing different catalyst promoters. It remains, however, to find efficient ways to separate the single-layer tubes from the soot and metal clusters in order to further characterize them and to assess their utility. As shown in this contribution, recent advances in HPLC separation of metallofullerenes now allow for detailed studies of the properties of endohedral fullerenes. EPR spectroscopy of $Sc_3@C_{82}$ reveals the interesting dynamical property of rapid reorientation of the Sc cluster inside the fullerene cage.

Acknowledgments

This research is partially supported by an NSF grant and by the Materials and Molecular Simulation Center, Beckman Institute, at Caltech. PvL acknowledges support by the Dutch Organization for Scientific Research (NWO). HCD acknowledges support from IBM and the Virginia Center for Innovative Technology.

References

1. S. Iijima and T. Ichihashi, *Nature* **363**, 603 (1993).
2. D. S. Bethune *et al.*, *Nature* **363**, 605 (1993).
3. Y. Saito *et al.*, *J. Phys. Chem. Solids* **54**, 849 (1993).
4. D. S. Bethune, R. D. Johnson, J. R. Salem, M. S. de Vries, and C. S. Yannoni, *Nature* **366**, 123 (1993).
5. R. S. Ruoff, D. C. Lorents, B. Chan, R. Malhotra, and S. Subramoney, *Science* **259**, 346 (1993); M. Tomita, Y. Saito, and T. Hayashi, *Jpn. J. Appl. Phys.* **32**, L280 (1993).
6. B. C. Guo, K. P. Kerns, and A. W. Castleman, Jr., *Science* **255**, 1411 (1992).
7. C.-H. Kiang, W. A. Goddard III, R. Beyers, J. R. Salem, and D. S. Bethune, *J. Phys. Chem.* **98**, 6612 (1994).
8. M. E. McHenry, S. A. Majetich, J. O. Artman, M. DeGraef, and S. W. Staley, *Phys. Rev.* **B49**, 11358 (1994).
9. S. Iijima, P. M. Ajayan, and T. Ichihashi, *Phys. Rev. Lett.* **69**, 3100 (1992).
10. M. Endo, *Chemtech* **18**, 568 (1988).
11. R. Saito, M. Fujita, G. Dresselhaus, and M. S. Dresselhaus, *Mat. Sci. Eng.* **B19**, 185 (1993).
12. S. Stevenson *et al.*, *Anal. Chem.* **66**, 2680 (1994).
13. S. Stevenson *et al.*, *Anal. Chem.* **66**, 2675 (1994).
14. H. Shinohara *et al.*, *Nature* **357**, 52 (1992); C. S. Yannoni *et al.*, *Science* **256**, 1191 (1992).
15. T. Kato, S. Suzuki, K. Kikuchi, and Y. Achiba, *J. Phys. Chem.* **79**, 13425 (1993).
16. P. H. M. van Loosdrecht *et al.*, *Phys. Rev. Lett.* **73**, 3415 (1994).